JOURNAL OF GUIDANCE, CONTROL, AND DYNAMICS
Vol. 23, No. 4, July–August 2000

Multiple On–Off Valve Control for a Launch Vehicle Tank Pressurization System

Perry W. Stout* and S. Antony Snell†
University of California, Davis, Davis, California 95616

Pressure control inside the propellant tanks of a pump-fed space launch vehicle is almost always a flight-critical task. Pressures are commonly controlled by admitting helium from high-pressure reservoirs into the propellant tank free volumes, or ullages. Controlled pressures must often satisfy the competing needs of engine net positive suction head, flight dynamic pressures, tank structural stability, and tank maximum expected operating pressure. Helium flows are usually governed by either regulators, proportional valves, or on–off solenoid valves implementing relay logic leading to control limit cycles. A new control scheme using on–off solenoid valves to approximate the performance of a proportional flow control valve has been synthesized for both stages of a space launch vehicle. This control system uses the same valves required by a competing limit cycle system but significantly improves system robustness in the face of system uncertainties, including initial engine outflow rates, ullage volumes, and helium-to-propellant heat transfer rates. Simulations indicate ullage pressures can be maintained within a 5-psi band at all times, despite the slow 25-Hz data communication rate assumed for this vehicle. Furthermore, the control logic provides a simple way to incorporate additional feedback signals such as engine pressure into the control loop to further improve tracking accuracy.

Nomenclature

A	= area
a	= acceleration
C_d	= discharge coefficient
c	= speed of sound
c_p	= specific heat capacity at constant pressure
c_v	= specific heat capacity at constant volume
d'	= inexact differential
$\mathrm{d}q/\mathrm{d}t$	= heat flux
E	= internal energy
e	= specific internal energy
F	= volumetric flow rate
g_c	= gravitation conversion constant, F/ma
h	= thermal convection coefficient; height
k	= thermal conductivity
m	= mass
$\dot{m}$	= mass flow rate
p	= pressure
R	= ideal gas constant; thermal resistance
T	= thermodynamic temperature
t	= thickness, time
V	= volume
v	= specific volume
W	= work
Z	= compressibility, pv/RT
γ	= ratio of specific heats, c_p/c_v
ρ	= density
σ	= relating to a control volume

I. Introduction

THE analyses shown in this paper are based on design efforts performed at Aerojet in Sacramento for the Kistler K-1 launch vehicle, a privately funded, two-stage space launch vehicle currently in development. The control system described herein does not necessarily represent the final control hardware or algorithms used on this vehicle because design requirements and hardware availability have changed during the program. However, these analyses do address most of the specific design issues encountered during Kistler vehicle development. Consequently, the results shown in this paper, and the software models used to generate them, remain relevant to this launch vehicle pressurization problem.

Large space launch vehicles almost always require active control of propellant tank internal pressures. To minimize vehicle weight, propellants are stored at low pressures in large, thin-walled tanks, then raised to engine operating pressures by high performance turbopumps. To ensure successful engine operation, propellants must enter the turbopumps above net positive suction head (NPSH) pressures to fluid prevent cavitation, a potentially catastrophic failure condition. Furthermore, tank internal pressures must always exceed external atmospheric pressures because thin tank walls are subject to buckling failure at low pressure differentials. Finally, tank pressures must often change in flight to hold tank stresses within design allowables because the loading environment changes with variations in dynamic pressure, vehicle acceleration, atmospheric pressure, and gravitational head of remaining propellants. A schematic of some of the loading conditions appearing on a typical propellant tank are shown in Fig. 1.

Tank pressures are controlled by admitting propellant-compatible gas into the tank free volume, or ullage, to replace propellants consumed by the engine(s). Helium is typically used because it is compatible with cryogenic propellants, and its low molecular weight provides high pressure per unit mass and volume, leading to minimum weight pressurization systems.

Surprisingly little information on these control systems can be found in the literature. This may reflect the proprietary nature of much of the work, the relatively small numbers of unique (as opposed to derivative) space launch vehicles, and their technological maturity, because most of the current inventory of U.S. space vehicles was developed in the 1950s and 1960s, when implementing closed-loop control systems was far more difficult than it is today. The most extensive reference is the Ref. 1 NASA technical report, but the results are not directly applicable because the helium pressurant was heated (Kistler uses cold gas) and the initial ullage volume was set to 5%. (The Kistler value is 1%.)

Control hardware can take many forms. Systems with constant pressure level requirements can use regulators; systems with variable pressure requirements use proportional flow or on–off solenoid valves combined with loop closure hardware. Proportional valves typically use brushless dc motor/ball screw combinations to

Received 2 March 1999; presented as Paper 99-4085 at the AIAA Guidance, Navigation, and Control Conference, Portland, OR, 9–11 August 1999; revision received 7 December 1999; accepted for publication 9 December 1999.

*Ph.D., Department of Mechanical and Aeronautical Engineering. Senior Member AIAA.

†Assistant Professor, Department of Mechanical and Aeronautical Engineering. Senior Member AIAA.

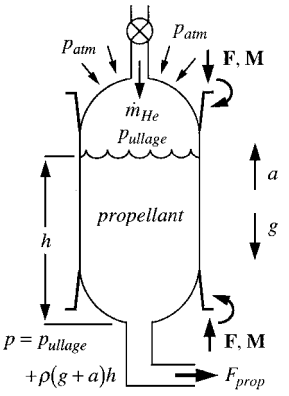

Fig. 1 Ullage pressure control is required to maintain tank structural integrity in a complex loading environment.

position a proportional actuator and require analog command inputs. Solenoid valves respond to higher power dc inputs; 2-A, 28-V circuits are typical. Backup control hardware is often provided to mitigate in-flight failures; however, in these analyses only control of primary actuators is considered.

Loop closure hardware typically includes either dual or triply redundant strain gauge-type pressure transducers, a communications bus, low-pass antialiasing filters, 12-bit A/D conversion hardware, dual or triplex processors with cross channel data links, and output driver circuits. The effects of sensor fault detection processes, sensor noise, A/D conversion, processor failure, and processor output selection are beyond the scope of these analyses, whereas the effects of antialiasing filters, sensor read delays, and computation delays are included.

II. Typical System Requirements

A simplified pressurization system schematic for a liquid oxygen (LOX)–rocket propellant-1 (RP-1) fueled booster rocket based on the Kistler K-1 first stage [also known as the launch assist platform (LAP)] is shown in Fig. 2. Helium is stored in 11 graphite fiber composite overwrap bottles at pressures up to 6000 psia (41.4 MPa), and initial temperatures of 50–90°F (283–305 K), with specific values of 6000 psia and 70°F used in simulation. Bottle heaters are not used in this system, and as a result helium gas temperatures in the storage bottles often drop below −172°F (160 K) at the end of simulation. Ullage pressure requirements vary depending on flight phase; controlled pressures range from 42–26 psia (290–179 kPa) for the LOX tank and 36–21 psia (248–145 kPa) for the RP tank.

Tank volumes for this investigation are 4580 ft^3 (129.7 m^3) for the LOX tank and 2607 ft^3 (73.8 m^3) for the RP. Initial ullage of 1% (45.8 and 26.07 ft^3 for LOX and RP, respectively) is also assumed.

Model pressure command histories, along with NPSH and tank structural limits, are shown in Figs. 3 and 4. Command histories may be provided by either preplanned lookup tables or by outputs from onboard trajectory computations.

Control valves must provide sufficient helium flow to replace propellant outflows of 34 ft^3/s (0.963 m^3/s) for LOX and 18.3 ft^3/s (0.518 m^3/s) for RP (52.3 ft^3/s total) at all supply pressures, a condition requiring large total orifice area. Control valves must also provide low flows to maintain accurate pressures when ullage volumes are small, helium supply pressures are at maximum, and engine flows are zero, a condition requiring fast valves with small orifices. To meet these competing objectives, multiple on–off solenoid valves are used as shown in Fig. 2. Each solenoid valve provides a fixed effective flow area $C_d A$, and in combination these valves provide a wide range of flows as needed to meet mission requirements.

Control valves require finite time to open and close. A maximum delay time of 30 ms is specified for all valve actuations. The control system must operate in the presence of high heat transfer rates to the LOX tank and moderate heat transfer rates to the RP tanks because initial tank wall temperatures and propellant bulk temperatures are −320°F (78 K) for LOX and −30°F (239 K) for RP. Furthermore, the control system must perform over a range of convective heat transfer coefficients to ensure robustness because heat transfer coefficients are rarely well known a priori.

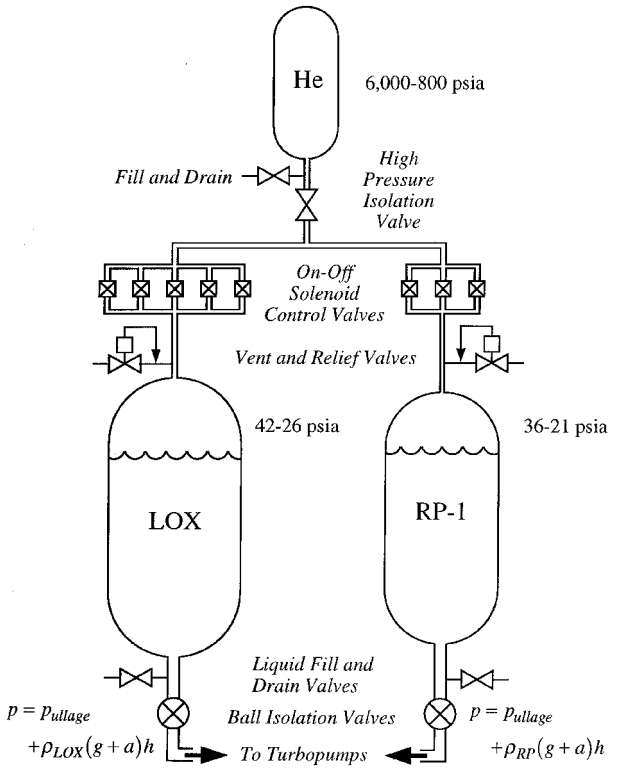

Fig. 2 Pressurization system uses on–off solenoid valves to control helium flows into main propellant tanks.

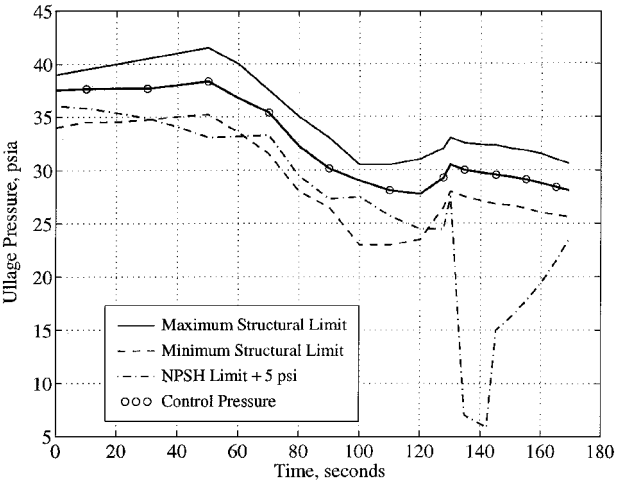

Fig. 3 LOX pressure command must fall within narrow band.

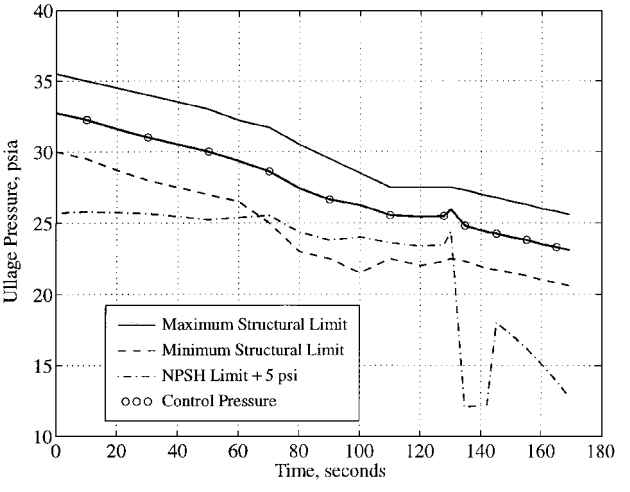

Fig. 4 RP control constraints are similar to LOX.

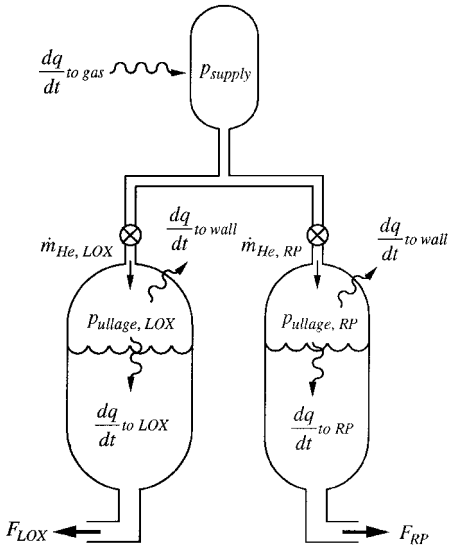

Fig. 5 Dynamic model computes helium mass and pressures in three separate regions.

Finally, the control system is implemented digitally. Vehicle system trade studies led to a low communications bus rate of 25 Hz, whereas selected processing equipment exhibits 12-ms analog input read delays and 16-ms computation delays. This loop closure rate is much lower than is generally desirable because it is quite close to the control system bandwidth; as a result these delays must be considered in the control design because they can measurably affect tracking accuracy and control loop robustness.

III. Dynamic Modeling

The pressurization system control model is based on a first law of thermodynamics analysis of energy flow in and out of three separate, uniform regions: the two ullage volumes and the high-pressure helium reservoir.[2] A schematic for dynamic modeling is shown in Fig. 5. The modeling process yields a linked set of eight nonlinear first-order state equations:

$$\frac{\mathrm{d}p_{\text{supply}}}{\mathrm{d}t} = \frac{1}{V_{\text{supply}}c_v}\left(\frac{m_{\text{supply}}RZ^2 + p_{\text{supply}}V_{\text{supply}}Z_T}{m_{\text{supply}}(Z - p_{\text{supply}}Z_P)}\right)\frac{\mathrm{d}q}{\mathrm{d}t} - \dot{m}_0\left(\frac{(c_v + ZR)m_{\text{supply}}Z + p_{\text{supply}}V_{\text{supply}}Z_T}{m_{\text{supply}}(Z - p_{\text{supply}}Z_P)}\right)\left(\frac{p_{\text{supply}}}{m_{\text{supply}}c_v}\right) \tag{1}$$

$$\frac{\mathrm{d}p_{\text{ullage, LOX}}}{\mathrm{d}t} = \frac{(\gamma-1)}{V_{\text{ullage, LOX}}}\dot{m}_{i,\text{LOX}}\left(\frac{c_v + RZ}{RZ}\right)\frac{p_{\text{supply}}V_{\text{supply}}}{m_{\text{supply}}} - \frac{\gamma p_{\text{ullage, LOX}}}{V_{\text{ullage, LOX}}}F_{\text{LOX}} + \frac{(\gamma-1)}{V_{\text{ullage, LOX}}}\frac{\mathrm{d}q}{\mathrm{d}t}_{\text{LOX}} \tag{2}$$

$$\frac{\mathrm{d}p_{\text{ullage, RP}}}{\mathrm{d}t} = \frac{(\gamma-1)}{V_{\text{ullage, RP}}}\dot{m}_{i,\text{RP}}\left(\frac{c_v + RZ}{RZ}\right)\frac{p_{\text{supply}}V_{\text{supply}}}{m_{\text{supply}}} - \frac{\gamma p_{\text{ullage, RP}}}{V_{\text{ullage, RP}}}F_{\text{RP}} + \frac{(\gamma-1)}{V_{\text{ullage, RP}}}\frac{\mathrm{d}q}{\mathrm{d}t}_{\text{RP}} \tag{3}$$

$$\frac{\mathrm{d}V_{\text{LOX ullage}}}{\mathrm{d}t} = F_{\text{LOX}} \tag{4}$$

$$\frac{\mathrm{d}V_{\text{RP ullage}}}{\mathrm{d}t} = F_{\text{RP}} \tag{5}$$

$$\frac{\mathrm{d}m_{\text{LOX ullage}}}{\mathrm{d}t} = \dot{m}_{\text{He LOX}} \tag{6}$$

$$\frac{\mathrm{d}m_{\text{RP ullage}}}{\mathrm{d}t} = \dot{m}_{\text{He RP}} \tag{7}$$

$$\frac{\mathrm{d}m_{\text{He supply}}}{\mathrm{d}t} = -(\dot{m}_{\text{He LOX}} + \dot{m}_{\text{He RP}}) \tag{8}$$

Here $Z_T \equiv \mathrm{d}Z/\mathrm{d}T$ and $Z_P \equiv \mathrm{d}Z/\mathrm{d}P$. Compressibility must be included to accurately compute helium usage because of the high gas storage pressures. National Bureau of Standards (NBS; now National Institute of Standards and Technology) helium compressibility data[3] were fit to a continuous function of two variables to create Z. This function is

$$Z(p,T) = (1.117\times10^{-10})p^2\sqrt{T} - (1.951\times10^{-5})p\sqrt{T} + (6.787\times10^{-4})\sqrt{T} - (1.993\times10^{-12})p^2T + (3.587\times10^{-7})pT - (1.512\times10^{-5})T - (1.735\times10^{-9})p^2 + (2.919\times10^{-4})p + 0.9927 \tag{9}$$

A plot of the Z function is shown in Fig. 6. The largest error between NBS data and the fitting function is 0.27%.

Propellant volumetric flow rates F_{LOX} and F_{RP} are set by engine flow demands and are initially highly variable. Typical LOX and RP flow functions for the three NK-33 engines (combined) used on the Kistler program are shown in Fig. 7. Note that these engine start transients are merely typical, and that the actual time required to establish full flow can vary by at least a factor of two. Mass flow between regions is governed by sonic flow equations. Above 1200 psia (8.27 MPa) the real gas equation is appropriate:

$$\dot{m}_{\text{real gas}} = C_d A \times \rho^*(p_0, T_0) \times C^*(p_0, T_0) \tag{10}$$

where density ρ and sonic velocity c are taken from NBS data. Note that $*$ refers to the sonic conditions in the valve orifice(s), and the subscript 0 refers to stagnation conditions in the high-pressure

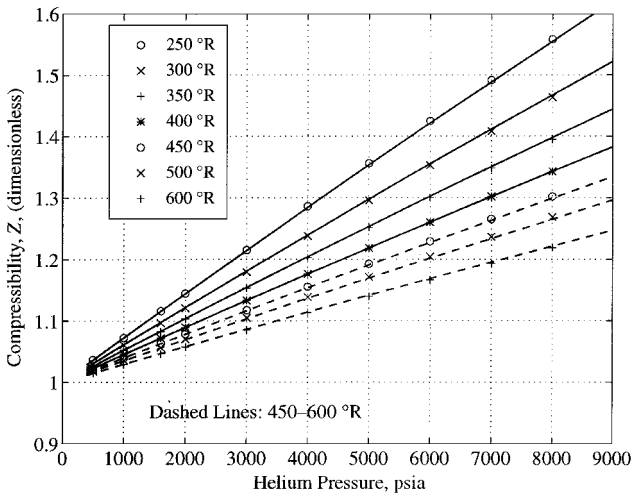

Fig. 6 $Z(p,T)$ function provides excellent fit to compressibility data.

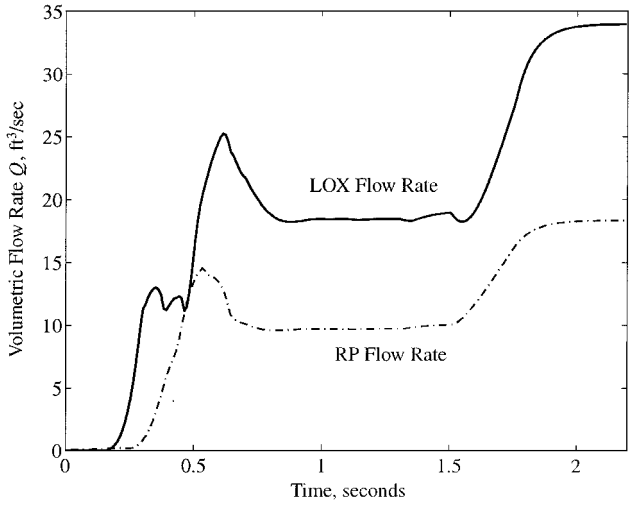

Fig. 7 Propellant flows are extremely variable at mission start.

reservoir. C_d is the discharge coefficient, with typical values ranging from 0.4 to 0.7, depending on valve type. $C_d = 0.6$ in this investigation.

Below 1200 psia the ideal gas sonic flow equation is used:

$$\dot{m}_{\text{ideal gas}} = C_d A \sqrt{\frac{p_{\text{supply}} m_{\text{supply}} \gamma g_c}{V_{\text{supply}}}} \left(\frac{2}{\gamma + 1}\right)^{[(\gamma+1)/2(\gamma-1)]} \tag{11}$$

The maximum error between $\dot{m}_{\text{real gas}}$ and $\dot{m}_{\text{ideal gas}}$ is only 4.0% at 6000 psia (41.4 MPa), with the ideal gas equation overpredicting true flow.

Two control inputs are $\dot{m}_{\text{He LOX}}$ and $\dot{m}_{\text{He RP}}$, with specific values set by $C_d A$. Schemes for setting $C_d A$ are discussed in Sec. IV, Control Loop Design.

Heat flux is the final input to the control model. Heat energy moves from the helium storage bottles to the helium supply and from the ullage volumes to the propellant tank walls and propellant free surfaces. Buoyant convection is assumed at gas/liquid and gas/solid interfaces, obeying the following law:

$$\frac{\mathrm{d}q}{\mathrm{d}t}_{\text{to surface}} = hA_{\text{surf}}\Delta T \tag{12}$$

Heat energy moves through the tankage by conduction, according to

$$\frac{\mathrm{d}q}{\mathrm{d}t}_{\text{conduction}} = -\frac{kA_{\text{tank}}\Delta T}{t_{\text{tank}}} \tag{13}$$

Both the liquid free surface areas and the exposed tank wall areas are determined by tank geometry and represented as functions of ullage volume. An infinite sink is assumed for heat transfer to the bulk propellants through the propellant free surfaces. Heat transfer to the tank walls, and from the high-pressure helium bottles to the helium

Table 1 Heat transfer coefficients vary with acceleration

Heat transfer condition	Acceleration, gs	h_{LOX} (Btu/h-ft^2-°F)	h_{RP} (Btu/h-ft^2-°F)
He gas to propellant free surface	all	1.08	0.80
He gas to tank wall	1	3.61	3.77
He gas to tank wall	3	4.75	4.97
He gas to tank wall	6	5.65	5.90
Bottle liner to He gas	all	h = 26	
Atmosphere to bottle overwrap	all	h = 0.88	
Atmosphere to tank exterior	all	h = 0	

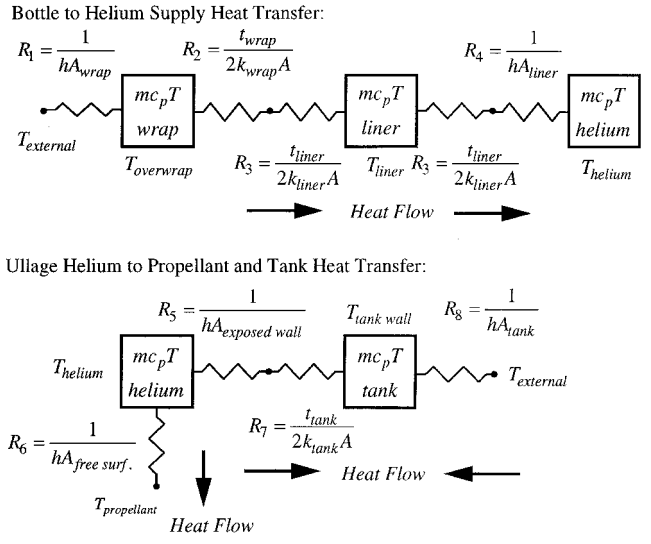

Fig. 8 Heat transfer model tracks energy flows through helium and propellant tankage.

supply assumes energy storage in the tank materials and conduction through tank walls. The two different thermal models are shown in Fig. 8, and the nominal convection coefficients are shown in Table 1.

The zero value for heat transfer coefficient from the atmosphere to tank exterior is conservative and reflects the possibility of operating the control system at high altitude near zero atmospheric pressures. In contrast the atmosphere-to-bottle-overwrap heat transfer coefficient reflects development test data and the possibility of operating the helium bottles in a pressurized interstage.

IV. Control Loop Design

System identification was the first step in the ullage pressure control loop design. A linearized model of some fidelity was required to illuminate control issues and suggest compensation strategies.

Examine the ullage pressure state equations (2) and (3). Here the ullage subscript has been dropped from p and V to improve readability and the helium flow term expanded to show its functional dependence:

$$\frac{\mathrm{d}p}{\mathrm{d}t} = \frac{(\gamma-1)}{V} C_d A \rho^*_{\text{supply}}(p_0, T_0) c^*_{\text{supply}}(p_0, T_0) \times \left(\frac{c_v + RZ}{RZ}\right) \frac{p_{\text{supply}} V_{\text{supply}}}{m_{\text{supply}}} - \frac{\gamma p}{V} F + \frac{(\gamma-1)}{V}\frac{\mathrm{d}q}{\mathrm{d}t} \tag{14}$$

The LOX and RP equations are only weakly linked through the helium reservoir states p_{supply} and m_{supply}. Consequently, the LOX and RP systems can be treated as a pair of single input/single output (SISO) systems rather than a more complex multi-input/multi-output (MIMO) system, greatly simplifying control system design. Whereas the pressure equation has a single control input ($C_d A$), $\mathrm{d}p/\mathrm{d}t$ takes one of two forms, depending on propellant volumetric flow rate F. During propellant fill and prelaunch operations $F \cong 0$, and the pressure equation becomes

$$\frac{\mathrm{d}p}{\mathrm{d}t} = \frac{K_1}{V} C_d A + \frac{(\gamma-1)}{V}\frac{\mathrm{d}q}{\mathrm{d}t} \tag{15}$$

where K_1 is defined as

$$K_1 = (\gamma-1)\rho^*_{\text{supply}}(p_0, T_0) c^*_{\text{supply}}(p_0, T_0) \times \left(\frac{c_v + RZ}{RZ}\right) \frac{p_{\text{supply}} V_{\text{supply}}}{m_{\text{supply}}} \tag{16}$$

The Laplace transform becomes

$$p(s) = (K_1/Vs) C_d A(s) + [(\gamma-1)/Vs]\dot{q}(s) \tag{17}$$

The transfer function between the control input $C_d A$ and the ullage pressure is an integrator with a crossover frequency set by ullage volume V and gain K_1. The heat transfer rate $\mathrm{d}q/\mathrm{d}t$ can be treated as a disturbance input. Its transfer function is also an integrator, indicating that the effect of this disturbance is cumulative. The pressure rise rate is governed by the magnitude of $C_d A$, whereas pressure decay occurs whenever $\mathrm{d}q/\mathrm{d}t$ is negative, the usual case in both tanks when propellants are present. Note that the V dependence of Eq. (15) changes the crossover frequency by a factor of 100 during tanking.

In flight, the character of the pressure equation changes to

$$\frac{\mathrm{d}p}{\mathrm{d}t} = -\frac{\gamma F}{V} p + \frac{K_1}{V} C_d A + \frac{(\gamma-1)}{V}\frac{\mathrm{d}q}{\mathrm{d}t} \tag{18}$$

and the effective control input transfer function becomes

$$\frac{p}{C_d A}(s) = \frac{K_1/V}{s + (\gamma F/V)} \tag{19}$$

a variable first-order lag, with break frequency set by both F and V and the bandwidth defined by K_1 and V.

Simple constant coefficient proportional-integral-derivative (PID) control structures are generally sufficient to control these

plants even with the wide range of bandwidth experienced during the mission, as long as linear actuators are available to produce $C_d A$. However, this control system is limited to on–off solenoid valves to produce $C_d A$ and therefore requires an alternative control strategy.

Conventional ullage pressure control systems rely on relay control sensing the sign of pressure error combined with hysteresis to produce stable limit cycles. Rather than supply a single valve with sufficient area to handle all flow demands, these systems provide multiple on–off valves to limit tracking errors. Valves are enabled, and disabled, open-loop according to carefully constructed mission schedules. Relay schemes currently fly on Atlas–Centaur, and remain a prime candidate for the Kistler control algorithm.

However, multiple on–off valves can also be used to create multilevel controllers as approximations to proportional valves, with up to $2^{n\ \text{valve}}$ separate levels. For example, the $C_d A_{\text{desired}}$ to $C_d A_{\text{delivered}}$ relationship for the three-valve RP actuator is shown in Fig. 9.

The delivered valve flow areas, control system switch points, and hysteresis values are shown in Tables 2 and 3. Hysteresis is still appropriate to prevent valve chatter when $C_d A_{\text{desired}}$ falls near a switch point.

The structure of the complete control loop is shown in Fig. 10.

Bandwidth Considerations

Placing numerical values in Eq. (17) shows that the initial open-loop system bandwidth is high; approximately 3100 psi/in^2-s. Because the closed-loop bandwidth must be set well below the Nyquist frequency, which is just 78.5 rad/s (12.5 Hz), the compensator gain will be much less than one. As a result, sensor noise amplification at the control input will be negligible and the open-loop system bandwidth does not constrain the closed-loop design.

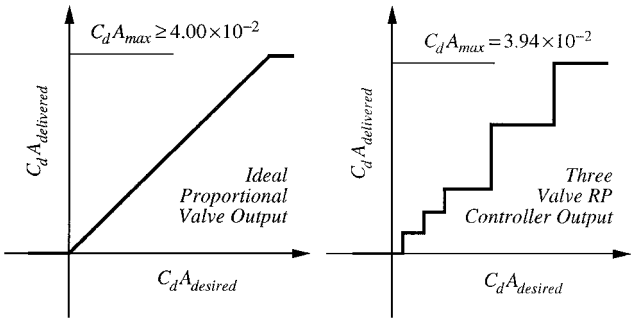

Fig. 9 RP three-valve actuator assembly provides five distinct flow levels.

The second consideration is disturbance rejection capability. The effects of engine start appear as a strong output disturbance in Eq. (19) as F moves rapidly from zero to full flow. Heat transfer effects are generally smaller, though heat transfer can cause significant control problems if the rush of incoming helium disturbs the propellant free surface and sprays LOX throughout the ullage volume, creating huge initial heat transfer coefficients. This quenching phenomenon was not explicitly considered in the design and in some circumstances can become the dominant disturbance. The narrow, 5-psia control band requires a high bandwidth to process out pressure errors quickly, making an initial system bandwidth of 20 rad/s or higher desirable. The third consideration is phase delay. Valves require 30 ms to open and close, the processing unit takes 12 ms to read values and 16 ms to generate command outputs, and the sampling system operates at 25 Hz. Assuming the effective delay of a zero-order hold is $T_s/2$, the total system delay is 78 ms. For this delay phase lag reaches 10 deg at 2.2 rad/s, 30 deg at 6.7 rad/s, and 60 deg at 13.4 rad/s.

The fourth consideration is valve schedule. Each valve set forms a multilevel controller and will generate limit cycles for certain combinations of system states; fewer valves lead to higher amplitude limit cycles. The amplitude of a limit cycle is an unavoidable

Table 2 LOX control valves provide 10 different flow levels

Valve combination	$C_d A$ provided	$C_d A$ switch level	Hysteresis
1	2.5112×10^{-3}	1.2556×10^{-3}	±.0001
2	6.6732×10^{-3}	4.5922×10^{-3}	±.0002
1,2	9.1844×10^{-3}	7.9288×10^{-3}	±.0002
3	1.3619×10^{-2}	1.1402×10^{-2}	±.0002
1,3	1.6130×10^{-2}	1.4874×10^{-2}	±.0002
2,3	2.0292×10^{-2}	1.8211×10^{-2}	±.0006
4	4.5286×10^{-2}	3.2789×10^{-2}	±.0004
3,4	5.8905×10^{-2}	5.2095×10^{-2}	±.0006
1,2,3,4	6.8089×10^{-2}	6.3497×10^{-2}	±.0006
1,2,3,4,5	1.8590×10^{-1}	1.2699×10^{-1}	±.0010

Table 3 Three RP control valves provide five different flow levels

Valve combination	$C_d A$ provided	$C_d A$ switch level	Hysteresis
1	3.1686×10^{-3}	1.5843×10^{-3}	0
2	6.7858×10^{-3}	4.9772×10^{-3}	0
1,2	9.9545×10^{-3}	8.3701×10^{-3}	0
3	2.9452×10^{-2}	1.9703×10^{-2}	±.0010
1,2,3	3.9407×10^{-2}	3.4430×10^{-2}	±.0010

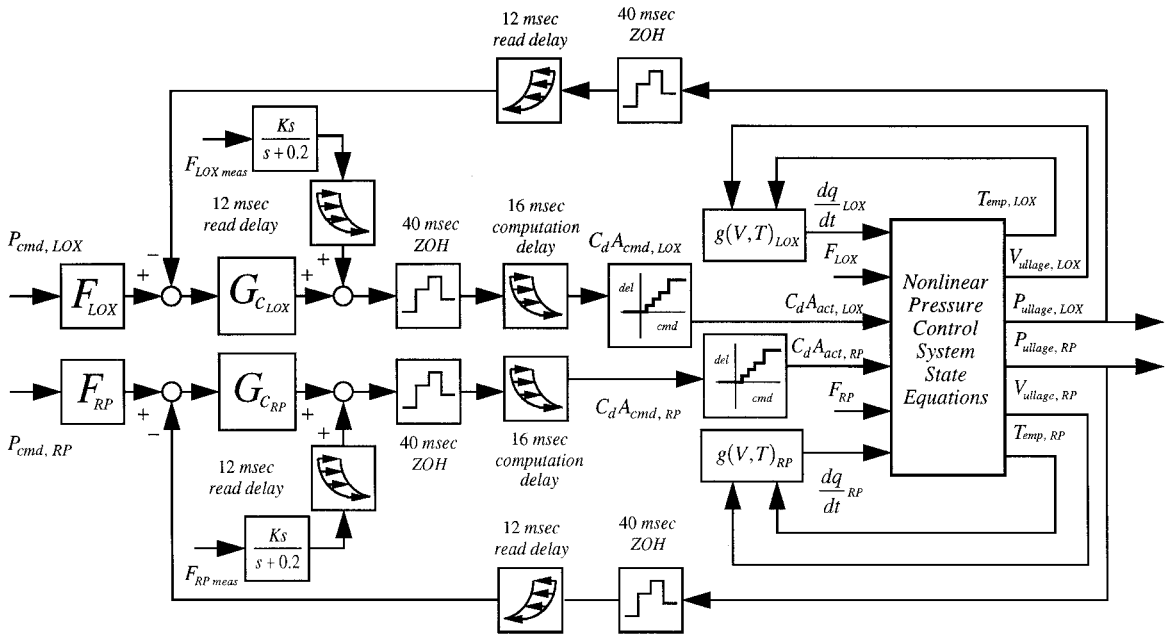

Fig. 10 Control loop incorporates command prefilters and flow rate feed forward.

tracking error; as a result larger amplitude limit cycles require higher accuracy, high-bandwidth controllers to hold pressures within fixed control limits.

Controller bandwidth requirements resulting from tracking accuracy needs and existing system phase delays are in direct conflict. Delivered control system performance is, therefore, primarily a compromise between these two constraints.

Control Structures

The prefilters shown in the left-hand side of Fig. 10 are included to prevent pressure overshoots when setpoints change. The same second-order filter is used on both tanks:

$$F(s) = 9/[s^2 + 1.4(3)s + 9] \tag{20}$$

Antialiasing filters are required at the A/D conversion interface and are, therefore, part of the control loop. The limited sampling rate also affected filter selection: A second-order filter with a relatively high break frequency was selected to minimize the effects of filter phase lag in the control loop. The antialiasing filter is

$$G_{A/D}(s) = 80^2/[s^2 + 1.4(80)s + 80^2] \tag{21}$$

The compensators are simple proportional-integral (PI) structures with zeros at 1 rad/s and variable gains. The huge change in bandwidth experienced during the mission leaves constant controller systems marginally stable after 115 s and allows pressure excursions outside the control band when proportional actuators are used. Scheduling the controller gain inversely with helium supply pressure solves this problem. The compensators including supply pressure feedback are

$$G_{c,\mathrm{LOX}}(s) = \frac{6000}{p_{\mathrm{supply}}} \times \frac{0.005(s+1)}{s} \tag{22}$$

$$G_{c,\mathrm{RP}}(s) = \frac{6000}{p_{\mathrm{supply}}} \times \frac{0.002(s+1)}{s} \tag{23}$$

Both integrators include antiwindup features to prevent excessive pressure excursions when the actuators enter saturation. Furthermore, the controllers are actually implemented in simulation as z-domain transfer functions by using Tustin's transformation with $T_s = 40$ ms. The transformed compensators are

$$G_{c,\mathrm{LOX}}(z) = \frac{6000}{p_{\mathrm{supply}}} \times \frac{(0.0051z - 0.0049)}{(z-1)} \tag{24}$$

$$G_{c,\mathrm{RP}}(z) = \frac{6000}{p_{\mathrm{supply}}} \times \frac{(0.00204z - 0.00196}{(z-1)} \tag{25}$$

Finally, the engine chamber pressure signal is injected downstream of the loop compensator. Because chamber pressure is directly proportional to engine flow rate, this signal provides an indication of ullage volume increase and helps improve tracking accuracy. A washout filter is used to turn off this signal after engine flows reach steady state:

$$F_c(s) = Ks/(s + 0.2) \tag{26}$$

or, implemented as a z-domain transfer function

$$F_c(z) = \frac{K(z-1)}{1.004z - 0.996} \tag{27}$$

Here K is the undetermined proportionality constant between chamber pressure and propellant flow rate.

The controller design can be assessed on the Nichols chart. Compensated transfer functions representing the LOX system just before engine start, just after reaching engine steady state, and just before engine shutdown are shown in Fig. 11. Two versions of the engine shutdown loop transmission are shown, one with, and one without, the scheduled gain.

The first observation is that all four loop transmissions indicate closed-loop stability even with the constant gain version of the compensator, despite the huge range in plant properties between prestart and engine shutdown. The second feature of these functions are the undesirable close approaches to the -1 point at 0 dB, -180 deg. For the prestart and engine running functions, the conflict between high bandwidth for tracking and system phase lag becomes apparent. Phase lag from system delays becomes substantial above 20 rad/s. Because the prestart and engine running dynamic models have crossover frequencies near 20 rad/s, robust stability is adversely affected by these unavoidable delays. Improved robustness at startup is impossible without reducing system delays or increasing initial ullage volumes.

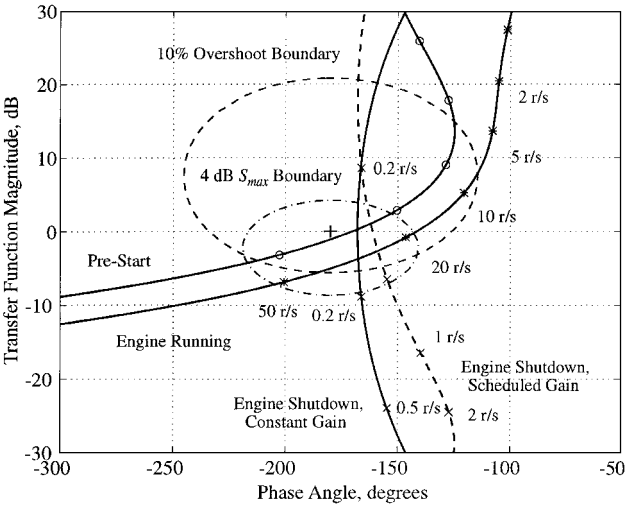

Fig. 11 LOX controller appears stable from engine start to shutdown.

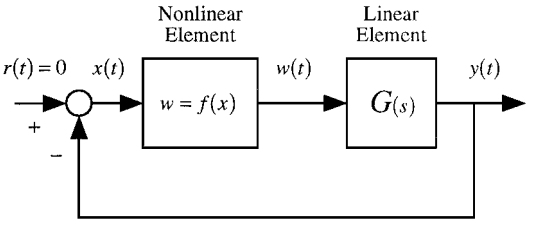

Fig. 12 Describing function method applies to systems with a single nonlinearity.

Although loop properties improve dramatically shortly after engine start, they degrade again when the crossover frequency drops below the zero at 1 rad/s. At engine shutdown the crossover frequency lies below 0.12 rad/s for the unscheduled compensator and provides just 12-deg phase margin. This marginally stable design provides poor command following; as a result ullage pressures fall outside the control band beyond 115 s when an ideal proportional actuator is used. The variable gain raises the crossover frequency at shutdown to 0.33 rad/s, thereby recovering some of the phase lead benefits of the zero at 1 rad/s. Phase margins improve 7 deg, and pressure command tracking errors return to the ±2.5-psia error band for the ideal actuator.

V. Describing Function Analysis

The Nichols chart analysis shown in Fig. 11 predicts a stable closed loop using a fully reversible, proportional valve. However the on–off solenoid valves selected to control helium flows between reservoirs provide only a few discrete flow levels into, and none out of, the propellant tanks. This single-sided nonlinear actuator will almost certainly generate control system limit cycles.

Describing function analysis[4] can be used to predict the magnitude and frequency of these limit cycles. Although the method is approximate, it generally provides good results when the controlled system behaves like a low-pass filter, as the ullage pressurization system does.

Describing functions can be applied to any system where the nonlinearity can be represented as an input–output relationship in an otherwise linear control loop, as shown in Fig. 12, subject to the

condition that the nonlinearity is odd and time invariant. Although it appears the solenoid valve set violates the first condition, it becomes a symmetric actuator during operation when maintaining $dp/dt = 0$, where a steady outflow F requires positive $C_d A$.

Describing function analysis is well known; see for example Slotine and Li[4] and Mohler.[5] Limit cycles are predicted whenever the open-loop transfer function $G(s)$ from Fig. 12 and the negative inverse of the describing function $N(A, \omega)$ are equal:

$$G(j\omega) = -1/N(A, \omega) \tag{28}$$

Note that the describing function is usually independent of frequency for most common engineering nonlinearities.

The real part of the LOX controller describing function is shown in Fig. 13. Note the separate peaks in $N(A)$ for each distinct value of $C_d A$ provided. Above the switchpoint $C_d A = 0.127$, the describing function declines as the actuator enters saturation at $C_d A = 0.186$.

A plot of $-1/N(A)$ and $G(s)$ in the s plane can be used to predict the magnitude and frequency of limit cycles. Figure 14 shows plots of $G(s)$ just before engine start, just after engine start, and before engine shutdown. Intersections occur at frequencies of 14.5, 13.5, and 0.41 rad/s (2.3, 2.1, and 0.065 Hz) at amplitudes of $C_d A = 0.079$, 0.0316, and 0.0357 in.^{2}. The limit cycle predicted to occur before engine start does not appear, mainly because the control valve assembly violates the odd function requirement when there is no propellant outflow. The describing function method does a good job of predicting the initial cycling behavior, accurately predicting both the existence and period of a limit cycle when the engine start disturbance sends a broad band of frequencies into the control system.

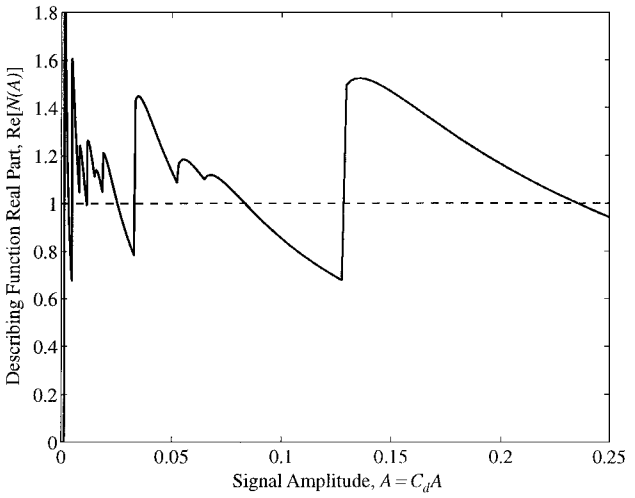

Fig. 13 LOX describing function output stays near unity.

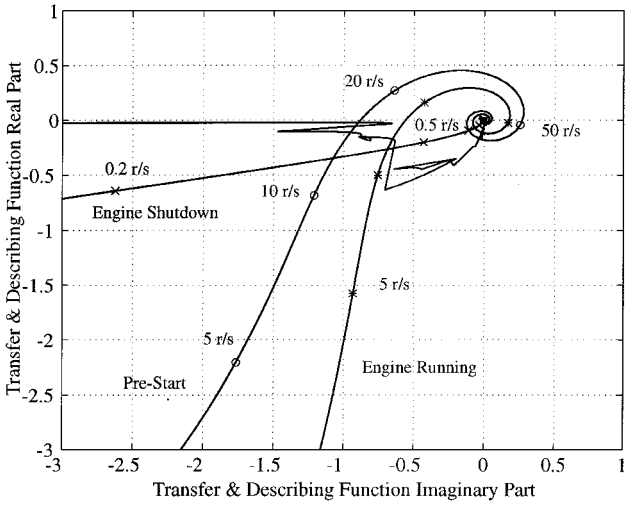

Fig. 14 Intersections of $G(s)$ and $1/N(A)$ predict limit cycle frequencies.

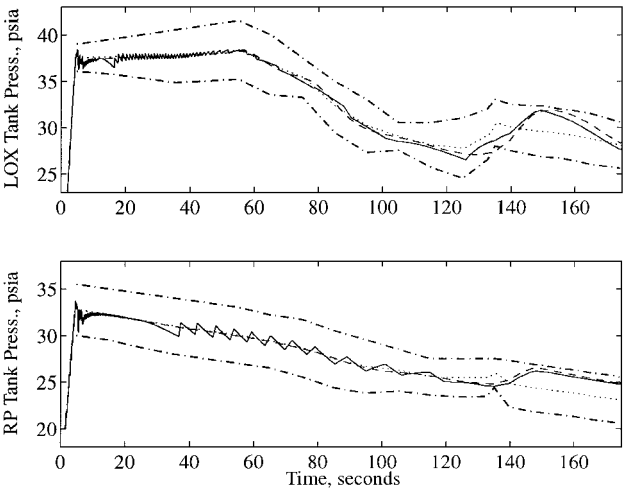

Fig. 15 Constant gain compensator tracks poorly after 115 s.

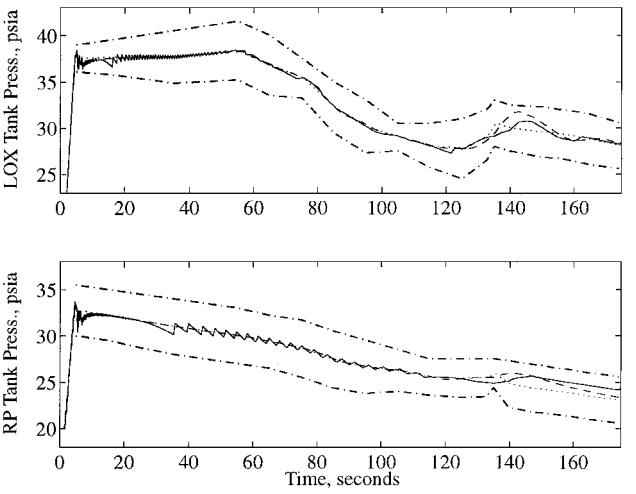

Fig. 16 Satisfactory performance provided by scheduled compensator.

VI. Simulations and Results

Simulations were performed with both a proportional valve and the multivalve controller, using the same compensator in both instances. Simulations are shown for both actuators to highlight the effectiveness of the multivalve scheme compared to an ideal proportional actuator and because the control loop was designed using a linear actuator. The proportional valve was modeled as a second-order system with $\omega_n = 30$ rad/s and $\zeta = 0.6$. Figure 15 shows plots of LOX and RP pressures for both the multivalve controller (solid lines) and the proportional valve (dashed lines) with a constant gain compensator. The effects of poor phase margin late in the mission are apparent as both traces approach the control limits after 115 s, with the LOX proportional valve trace actually falling outside the control envelope at 135 s. Note that the initial pressures are 20 psia in both tanks and that both tanks are commanded to startup pressure at $t = 1$ s before engine start at $t = 5$ s.

A second set of simulations is shown in Fig. 16, where the constant gain compensators are replaced by the scheduled gain algorithms. The late mission command tracking improves substantially, as both the proportional valve and the multivalve controller system traces remain well within the ±2.5-psia control band.

An expanded view of the first 15 s shown in Fig. 17 reveals the high control activity level during the start transient, where engine flows go from zero to full in just 2.2 s. Engine feedforward is essential for the compensator to meet tracking requirements, especially on the LOX side where NPSH requirements have narrowed the initial tracking band from 5 to just 2.93 psia.

Helium supply pressure and all system helium temperature histories are shown in Fig. 18.

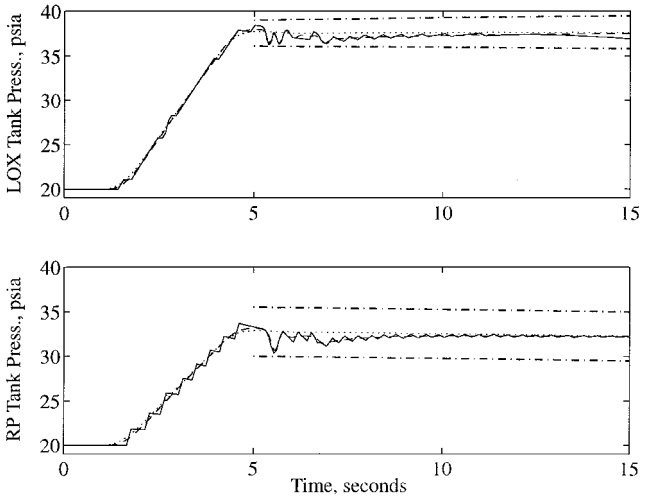

Fig. 17 Control system shows high activity during engine start.

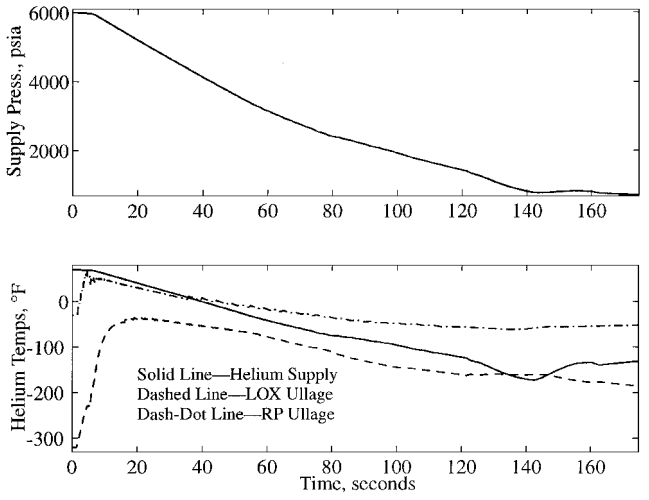

Fig. 18 Helium supply pressure and all helium temperatures vary widely.

VII. Conclusions

Using multiple on–off solenoid valves to approximate the performance of proportional flow valves in a launch vehicle ullage pressure control system is an attractive solution. PI control structures combined with a simple variable gain set by another feedback signal provide excellent robustness over the entire range of operating conditions and can eliminate the open-loop control features found in conventional limit-cycle systems. The system examined held ullage pressures within a 5-psia and tighter operating band, even during a difficult engine startup period when control requirements are most stringent and despite a low initial ullage volume of 1% and a slow 25-Hz sampling rate. Furthermore, solenoid operated valves are generally much less expensive than proportional valves, and integrate well with modern digital flight computation and control equipment.

Finally, it is revealing to examine helium supply pressure and all system helium temperature histories (Fig. 18) because these states determine helium specific volume in the tank ullages. The wide range of supply pressures and temperatures tolerated by the control system are a direct measure of system robustness.

Still, all control systems have limits. The minimum controllable ullage volume, and the effects of helium quench on start transients remain to be determined. The precise magnitudes of these effects will determine the minimum allowable sampling rates and maximum allowable system delays required to implement a completely closed-loop ullage pressure control system.

Much future work remains to be done on the multiple on–off solenoid valve controller design. Control system features described earlier in the paper (sensor fault detection processes, sensor noise, A/D conversion, processor failure, and processor output selection) but not included in these analyses must be incorporated. The dynamic model must evolve to reflect current launch vehicle configurations and hardware performance, especially for valves. The compensation algorithm should be implemented in fixed-point arithmetic, to reflect the behavior of actual flight hardware, and the model must be run through a Monte Carlo analysis to thoroughly test system robustness before approving this scheme for flight.

Appendix: Modeling the Ullage Pressure Control Problem

By the first law for a variable volume open system, the rate of heat and work added to a control volume equals the sum of the rate of change of its internal energy, the $p\,\mathrm{d}V$ work done by the gas, and the mass-enthalpy transport across system borders:

$$\frac{\mathrm{d}'Q}{\mathrm{d}t} + \frac{\mathrm{d}'W_{\text{ext}}}{\mathrm{d}t} = \left(\frac{\mathrm{d}E}{\mathrm{d}t}\right)_\sigma + \left(\frac{p\,\mathrm{d}V}{\mathrm{d}t}\right)_\sigma + \dot{m}_0 h_0 - \dot{m}_i h_i \quad \text{(A1)}$$

where σ refers to the control volume in question, either the variable volume LOX or RP ullage or the fixed-volume, high-pressure helium reservoir. The symbol d' represents an inexact differential, reflecting that rates of change for heat and work are path dependent.

External work done on these reservoirs is zero, and each has just a single inlet or outlet, not both. The first law for an ullage reservoir can be rewritten as

$$\frac{\mathrm{d}E}{\mathrm{d}t} = \dot{m}_i h_i - \frac{p\,\mathrm{d}V}{\mathrm{d}t} + \frac{\mathrm{d}q}{\mathrm{d}t} \quad \text{(A2)}$$

where $\mathrm{d}'Q/\mathrm{d}t$ has been replaced with heat flux $\mathrm{d}q/\mathrm{d}t$ that will be replaced later by a heat transfer model.

The internal energy of helium over a wide range of temperatures and pressures can be expressed simply as

$$E = mc_v T \quad \text{(A3)}$$

where c_v is a constant, 596.6 ft · $\mathrm{lb}_f/\mathrm{lb}_m$ · °R (3212 J/kg · K) as computed from NBS data over a wide range of temperatures and pressures. Furthermore, the thermodynamic temperature T can be replaced with pressure and volume by the real gas relationship:

$$T = pV/mZR \quad \text{(A4)}$$

where Z is the compressibility factor, and R is the gas constant for helium, 386.3 ft · $\mathrm{lb}_f/\mathrm{lb}_m$ · °R (2078 J/kg · K). Substituting Eqs. (A3) and (A4) into Eq. (A2) forms

$$\frac{c_v}{R}\frac{\mathrm{d}}{\mathrm{d}t}\left(\frac{pV}{Z}\right) = \dot{m}_i h_i - \frac{p\,\mathrm{d}V}{\mathrm{d}t} + \frac{\mathrm{d}q}{\mathrm{d}t} \quad \text{(A5)}$$

At the low pressures found in the propellant ullages, $Z \cong 1$. Furthermore, because at low pressures $R = c_p - c_v$ and $\gamma = c_p/c_v$,

$$c_v/R = 1/(\gamma - 1) \quad \text{(A6)}$$

Substituting Eq. (A6) into Eq. (A5) and using the chain rule to expand the pV term yields

$$\frac{p}{\gamma - 1}\frac{\mathrm{d}V}{\mathrm{d}t} + \frac{V}{\gamma - 1}\frac{\mathrm{d}p}{\mathrm{d}t} = \dot{m}_i h_i - p\frac{\mathrm{d}V}{\mathrm{d}t} + \frac{\mathrm{d}q}{\mathrm{d}t} \quad \text{(A7)}$$

where $\mathrm{d}V/\mathrm{d}t$ is the change in ullage volume that is set by engine volumetric flow rates. Because engine flows are essentially independent of ullage pressures, $\mathrm{d}V/\mathrm{d}t$ becomes a control input F. Rearranging Eq. (A7) yields

$$\frac{\mathrm{d}p}{\mathrm{d}t} = \frac{(\gamma - 1)}{V}\dot{m}_i h_i - \frac{\gamma p}{V}F + \frac{(\gamma - 1)}{V}\frac{\mathrm{d}q}{\mathrm{d}t} \quad \text{(A8)}$$

Finally, the enthalpy of the incoming helium equals the enthalpy of the stored gas in the high-pressure supply because the flow process through the control valves is essentially adiabatic.

Specific enthalpy is defined as

$$h = e + pv = c_v T + pv \tag{A9}$$

where T, p, and v refer to the temperature, pressure, and specific volume in the supply reservoir. Eliminating T using Eq. (A4) from Eq. (A9) yields

$$h_i = c_v \frac{p_{\text{supply}} V_{\text{supply}}}{m_{\text{supply}} R Z_{\text{supply}}} + \frac{p_{\text{supply}} V_{\text{supply}}}{m_{\text{supply}}} = \left(\frac{c_v + RZ}{RZ}\right) \frac{p_{\text{supply}} V_{\text{supply}}}{m_{\text{supply}}} \tag{A10}$$

and the final ullage pressure equation becomes

$$\frac{\mathrm{d}p_{\text{ullage}}}{\mathrm{d}t} = \frac{(\gamma - 1)}{V_{\text{ullage}}} \dot{m}_i \left(\frac{c_v + RZ}{RZ}\right) \frac{p_{\text{supply}} V_{\text{supply}}}{m_{\text{supply}}} - \frac{\gamma p_{\text{ullage}}}{V_{\text{ullage}}} F + \frac{(\gamma - 1)}{V_{\text{ullage}}} \frac{\mathrm{d}q}{\mathrm{d}t} \tag{A11}$$

The compressibility factor Z has reappeared because the enthalpy term refers to conditions in the high pressure supply, not the ullages.

The pressure equation for the helium supply has a different form. Because the reservoir is constant volume, helium leaves the region, and compressibility must be considered as part of the equation of state. Equation (A5) becomes

$$\frac{c_v}{R} \frac{\mathrm{d}}{\mathrm{d}t}\left(\frac{pV}{Z}\right) = -\dot{m}_0 h_0 + \frac{\mathrm{d}q}{\mathrm{d}t} \tag{A12}$$

or, expanded,

$$\frac{V c_v}{R}\left(\frac{1}{Z}\frac{\mathrm{d}p}{\mathrm{d}t} - \frac{p}{Z^2}\frac{\mathrm{d}Z}{\mathrm{d}t}\right) = -\dot{m}_0 h_0 + \frac{\mathrm{d}q}{\mathrm{d}t} \tag{A13}$$

Z is a function of pressure and temperature. Therefore, by the chain rule,

$$\frac{\mathrm{d}Z}{\mathrm{d}t} = \frac{\mathrm{d}Z}{\mathrm{d}p}\frac{\mathrm{d}p}{\mathrm{d}t} + \frac{\mathrm{d}Z}{\mathrm{d}T}\frac{\mathrm{d}T}{\mathrm{d}t} \tag{A14}$$

Both $\mathrm{d}Z/\mathrm{d}p$ and $\mathrm{d}Z/\mathrm{d}T$ are computable from the Z function, whereas $\mathrm{d}T/\mathrm{d}t$ can be expressed in terms of pressure according to

$$\frac{\mathrm{d}T}{\mathrm{d}t} = \frac{\mathrm{d}}{\mathrm{d}t}\left(\frac{pV}{mRZ}\right) = \frac{V}{R}\left(\frac{1}{mZ}\frac{\mathrm{d}p}{\mathrm{d}t} - \frac{p}{mZ^2}\frac{\mathrm{d}Z}{\mathrm{d}t} - \frac{p}{Zm^2}\frac{\mathrm{d}m}{\mathrm{d}t}\right) \tag{A15}$$

After substituting Eq. (A15) into Eq. (A14) and rearranging, $\mathrm{d}Z/\mathrm{d}t$ becomes

$$\frac{\mathrm{d}Z}{\mathrm{d}t} = \left(\frac{mRZ^2(\mathrm{d}Z/\mathrm{d}p) + VZ(\mathrm{d}Z/\mathrm{d}T)}{mRZ^2 + (\mathrm{d}Z/\mathrm{d}T)pV}\right)\frac{\mathrm{d}p}{\mathrm{d}t} - \left(\frac{(\mathrm{d}Z/\mathrm{d}T)}{mRZ^2 + pV(\mathrm{d}Z/\mathrm{d}T)}\right)\frac{pVZ}{m}\frac{\mathrm{d}m}{\mathrm{d}t} \tag{A16}$$

Defining Z_p as $\mathrm{d}Z/\mathrm{d}p$, Z_T as $\mathrm{d}Z/\mathrm{d}T$, and setting $\mathrm{d}m/\mathrm{d}t = -\dot{m}_0$ creates the more compact form:

$$\frac{\mathrm{d}Z}{\mathrm{d}t} = \left(\frac{mRZ^2 Z_p + VZZ_T}{mRZ^2 + Z_T pV}\right)\frac{\mathrm{d}p}{\mathrm{d}t} + \left(\frac{Z_T}{mRZ^2 + pVZ_T}\right)\frac{pVZ\dot{m}_0}{m} \tag{A17}$$

Substituting Eq. (A17) into Eq. (A13) produces

$$\frac{Vc_v}{R}\left[\frac{mRZ(Z - pZ_p)}{Z\left(mRZ^2 + pVZ_T\right)}\right]\frac{\mathrm{d}p}{\mathrm{d}t} = -\dot{m}_0 h_0 + \dot{m}_0\left(\frac{Vc_v}{R}\right)\left(\frac{pZ_T}{mRZ^2 + pVZ_T}\right)\left(\frac{pV}{mZ}\right) + \frac{\mathrm{d}q}{\mathrm{d}t} \tag{A18}$$

or, after replacing h_0 with $(c_v + ZR)(pV/mZR)$,

$$Vc_v\left[\frac{mZ(Z - pZ_p)}{Z\left(mRZ^2 + pVZ_T\right)}\right]\frac{\mathrm{d}p}{\mathrm{d}t} = -\dot{m}_0\left(\frac{(c_v + ZR)mZ + pVZ_T}{mRZ^2 + pVZ_T}\right)\left(\frac{pV}{m}\right) + \frac{\mathrm{d}q}{\mathrm{d}t} \tag{A19}$$

Finally, $\mathrm{d}p/\mathrm{d}t$ for the helium supply becomes

$$\frac{\mathrm{d}p_{\text{supply}}}{\mathrm{d}t} = \frac{1}{V_{\text{supply}} c_v}\left(\frac{m_{\text{supply}} RZ^2 + p_{\text{supply}} V_{\text{supply}} Z_T}{m_{\text{supply}}(Z - p_{\text{supply}} Z_p)}\right)\frac{\mathrm{d}q}{\mathrm{d}t} - \dot{m}_0\left(\frac{(c_v + ZR)m_{\text{supply}} Z + p_{\text{supply}} V_{\text{supply}} Z_T}{m_{\text{supply}}(Z - p_{\text{supply}} Z_p)}\right)\left(\frac{p_{\text{supply}}}{m_{\text{supply}} c_v}\right) \tag{A20}$$

Acknowledgments

This work was sponsored by Aerojet and Kistler Aerospace Corporation. Contributions to this work were made by Chuck Limerick and Richard Bailey of Kistler Aerospace, Bryan Beaudette and Ed Bair of Aerojet, and Ichi Wakabayashi of Senior Flexonics/Ketema Division. The Aerojet Program Manager is Deborah Rickman and the Kistler Program Manager is Joe Cuzzupoli.

References

[1]"Volume II, Appendix G: Tank Pressurization Control System Study," *Propellant Tank Pressurization System Technology Program*, NASA TR NAS8-37666, Honeywell Corp. for Martin Marietta Manned Space Systems, Oct. 1990.

[2]Holman, J. P., "Energy Analysis in Open Systems," *Thermodynamics*, 4th ed., McGraw–Hill, New York, 1988, pp. 128–135.

[3]McCarty, R. D., "Thermophysical Properties of Helium-4 from 4 to 3000 R with Pressures to 15000 PSIA," National Bureau of Standards, TN 622, 1972.

[4]Slotine, J.-J. E., and Li, W., "Describing Function Analysis," *Applied Nonlinear Control*, Prentice–Hall, Upper Saddle River, NJ, 1991, pp. 157–188.

[5]Mohler, R. R., "Describing Function Method," *Nonlinear Systems—Volume 1, Dynamics and Control*, Prentice–Hall, Upper Saddle River, NJ, 1991, pp. 219–235.